Numerical Simulation of the Wicking Effect in Liner Systems

by T.-C. Jim Yeh[a], Amado Guzman[a], Rajesh Srivastava[b], and Philip E. Gagnard[c]

Abstract

Numerical simulations were carried out to investigate the capillary barrier effect and the wicking ability of multilayer earth liner systems. Two specific cases were studied: a two-layer liner composed of a fine- over a coarse-textured material, and a three-layer liner composed of a medium-textured material in between a fine- and a coarse-textured material. Results of the simulations show that a quadratic relationship exists between the thickness of the fine-textured material and the arrival time of the wetting front to the interface. At the time the wetting front reaches the interface, the width of the lateral spreading within the fine material is smaller than the thickness of this material. The lateral spreading and thickness are linearly related. The wicking ability of the different materials is more significant under relatively smaller infiltration rates and is controlled by the magnitude of the hydraulic diffusivity. For the two-layer liner the criteria of minimizing the vertical movement and maximizing the wicking effect within the fine-textured material conflict. A three-layer liner satisfies both of these criteria. The results for the three-layer system show that the medium-textured material has more superior wicking properties than the fine material does.

Introduction

Waste disposal facilities such as landfills, tailing ponds, and radioactive waste repositories in the U.S. commonly use multilayer liners to isolate industrial and municipal wastes from the accessible environment—aquifers, rivers, and the atmosphere. In general, these liners rely on low permeability media such as clays and man-made materials (e.g., flexible membrane liners, etc.) to contain the waste products (Geswein, 1975).

In some cases, the liner is constructed with a fine-textured earth material overlying a coarse-textured earth material. The coarse material is more permeable than the fine material under near saturated conditions. However, as the degree of saturation decreases (matric potential becomes more negative), the difference in conductivity between coarse and fine material becomes smaller. Beyond a threshold matric potential value, the coarse material can be less permeable than the fine material. Therefore, under very dry conditions (beyond the threshold matric potential value), the coarse-textured material can act as a capillary barrier to water in the fine-textured material until the moisture at the interface between the two materials builds up sufficiently to penetrate into the coarse material (Hillel, 1971).

Due to the capillary barrier effect, leachate penetrating the fine and less permeable material in a liner system tends to spread out laterally in the fine material after the wetting front advances to the interface between the fine and the coarse material. This lateral migration along the interface is called the "wicking effect." Past studies have substantiated that both effects, the capillary barrier and the wicking, occur in a soil system consisting of a layer of fine-textured material overlying a layer of coarse-textured material (Frind et al., 1977; Zaslavsky and Sinai, 1981; Johnson et al., 1983; McWhorter et al., 1983; Ross, 1990; Gagnard et al., 1993). Yeh et al. (1985) based on the result of a stochastic analysis proposed a liner system, consisting of multiple layers of fine and coarse materials, which enhances moisture dependent anisotropy of the system and thus, the wicking effect.

The State of California, for example, requires detection of waste constituents migrating from waste disposal facilities before they reach ground water (California Administrative Code, Title 23, Chapter 3, Subchapter 15, Article 15). A liner system consisting of a fine- over a coarse-textured material may be desirable because of the capillary barrier and the wicking effect. These effects enhance the lateral movement of water and solutes within the liner system in such a manner that facilitates collection and monitoring of leachates from the waste disposal facilities, using a relatively sparse sampling network. Furthermore, such an "early warning" has the advantage of detecting leachate migration long before it reaches the environment.

In this study, numerical simulations were performed to quantify the wicking abilities of five fine-textured materials

[a]Associate Professor and Graduate Student, respectively, Department of Hydrology and Water Resources, The University of Arizona, Tucson, Arizona 85721.

[b]Postdoctoral Research Associate, Department of Soil and Water Science, The University of Arizona, Tucson, Arizona 85721.

[c]Assistant Director, Waste Management of North America, Inc., 3003 Butterfield Road, Oak Brook, Illinois 60521.

Received January 1993, revised June 1993, accepted July 1993.

for a two-layer liner system and to evaluate the efficiency of a three-layer liner system. More specifically, the purpose of this modeling effort was: to quantify the effect of the thickness of the low conductivity layer on the lateral speading of the wetting front; to evaluate the effect of leakage rate on the lateral spreading; to develop a criterion for selection of the material that produces maximum wicking and minimizes the water movement through the liner; and finally, to examine the wicking effect of a three-layer system. It should be noted, however, that migration of some leachate solutions is not the same as that of water. Depending on the chemical composition of the liner and the leachate solutions, the hydraulic properties of its materials may be altered (Haxo et al., 1985). This study is limited to leachate solutions which migrate with water and does not include other constituents, such as dense nonaqueous phase liquids or reactive constituents. Also, the study focused on multilayer earth liners as opposed to synthetic materials.

Numerical Model

The numerical experiments discussed below are based on the numerical solution of the two-dimensional Richard's equation (Bear, 1972) for unsaturated flow:

$$\frac{\partial}{\partial x}\left[K(\Psi)\frac{\partial \Psi}{\partial x}\right]+\frac{\partial}{\partial y}\left[K(\Psi)\frac{\partial(\Psi+y)}{\partial y}\right]=C(\Psi)\frac{\partial \Psi}{\partial t} \quad (1)$$

where $K(\Psi)$ is the hydraulic conductivity (assuming isotropic in x and y directions); $C(\Psi)$ is the specific moisture capacity and is defined as $d\theta/d\Psi$ where θ is the volumetric moisture content; x is the horizontal coordinate; y is the vertical coordinate (positive upward); t is the time; and Ψ is the matric potential. Equation (1) is nonlinear in that the parameters K and C are strongly dependent on the matric potential, Ψ (a negative pressure under unsaturated conditions). The finite-element computer model, VSAFT2 (Yeh and Srivastava, 1990), was used to obtain the numerical solution of the above equation. This model is based on a Galerkin finite-element technique and an adaptive time stepping scheme, and utilizes both the Picard and Newton-Raphson approach for the nonlinear iterations (Istok, 1989). The code has been tested under various flow and transport situations and has been found to be quite robust and accurate, mass balance errors being typically less than 5% (Yeh et al., 1993).

The unsaturated hydraulic properties of all materials to be examined in the numerical experiments were assumed to be represented by the van Genuchten model. That is, the moisture content-matric potential relationship (water release curve) of the materials is given by

$$\theta(\Psi)=(\theta_s-\theta_r)\left[1+(-\alpha\Psi)^n\right]^{-m}+\theta_r \quad (2)$$

Similarly, the hydraulic conductivity-matric potential relationship is described by

$$K(\Psi)=K_s\frac{\left(1-(-\alpha\Psi)^{n-1}\left[1+(-\alpha\Psi)^n\right]^{-m}\right)^2}{\left[1+(-\alpha\Psi)^n\right]^{m/2}} \quad (3)$$

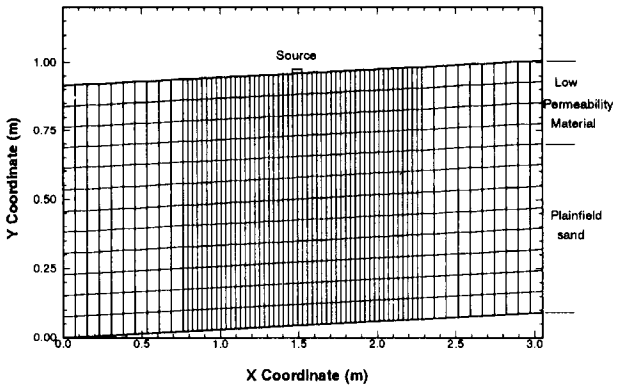

Fig. 1. Schematic representation of the simulated cross section.

where K_s is the saturated hydraulic conductivity. θ_s and θ_r are moisture content at saturation, and residual moisture content, respectively. α and n are parameters controlling the curvature of the relationships and $m = 1 - 1/n$. The moisture capacity term, $d\theta/d\Psi$, required in the numerical model is internally calculated in VSAFT2 by differentiating (2).

Two-Layer System

Description of the Physical Setting

Using VSAFT2, flow through several hypothetical two-layer liners consisting of a fine-textured material overlying a coarse-textured material was investigated. The liners were assumed to have a 3% slope as is typical for a leachate collection system. Vertical cross sections with dimensions of 3.05 meters in the horizontal and 0.91 meters in the vertical, as depicted in Figure 1, were used for most of the simulations. For illustration purposes, the thickness of the top, fine-textured layer was assumed to be 0.30 meters and that of the bottom, coarse-textured layer was 0.61 meters. The vertical dimension of the cross section was varied in some simulations to study the effect of liner unit thickness on lateral spreading of the wetting front.

Material Properties

Five low conductivity materials, Excel, Celite Slurry, Kiln Dust, Rock Creek, Celite Waste, with saturated hydraulic conductivity ranging from 1.80×10^{-6} to 7.32×10^{-4} m/hr (meters per hour) were selected as candidates for the fine-textured layer of the liner system. Plainfield sand, with a saturated hydraulic conductivity of 1.08 m/hr, was used as the coarse material for the bottom layer of the system. Actual hydraulic conductivities of these materials will depend on the in situ compaction and water content during liner construction. For this study, it was assumed that the sample density was representative of in situ conditions.

Laboratory determinations of the water release curves and the saturated hydraulic conductivity values for the five materials were conducted by the vadose zone monitoring laboratory at the University of California, Santa Barbara. Equation (2) was then fitted to the measured water content and matric potential data by using a nonlinear least-squares model (van Genuchten, 1978) to obtain the parameters (α, n, and θ_r) of the model. The water content and matric potential data for the Plainfield sand was obtained from a soil

Table 1. Hydraulic Properties for the Layers

Layer	K_{sat} (m/hr)	θ_{sat}	θ_{res}	α (m^{-1})	n
Excel	7.32×10^{-4}	0.95	0.413	1.090	1.832
Celite Slurry	1.50×10^{-4}	0.84	0.499	0.397	1.814
Kiln Dust	7.32×10^{-5}	0.72	0.192	1.070	2.305
Rock Creek	1.80×10^{-6}	0.395	0.325	1.070	2.425
Celite Waste	3.66×10^{-5}	0.98	0.640	0.512	3.130
Plainfield Sand	1.08	0.36	0.030	2.408	15.04

catalog (Mualem, 1976) and fitted in the same fashion as described above. Table 1 summarizes the model parameters for the six materials used in the simulations. Using these parameter values, hydraulic conductivity and matric potential curves for the six materials were generated with equation (3). Graphical representation of the volumetric water content and the hydraulic conductivity as a function of suction (absolute value of matric potential) for these materials are presented as Figures 2 and 3, respectively.

Initial and Boundary Conditions

Initial conditions for all the simulations in this study were assigned to represent a state of hydrostatic equilibrium with a uniform total-head distribution of -10 meters of water in the vertical cross section. This initial condition implies that there was no moisture movement in the liner before the occurrence of the leakage. The corresponding matric potential pressure, considering the slope of the system, varied from -10 meters in the lower left corner to -10.91 meters at the top right corner of the cross section. The volumetric water content of the layers for this initial matric potential distribution can be obtained by using the water release curves presented in Figure 2.

Boundary conditions of the liner system were assigned as follows: no-flow along the top, left, and right boundaries of the cross section and unit gradient conditions along the lower boundary. Point source leakage from the landfill to the liner was treated as a constant flow rate at the three

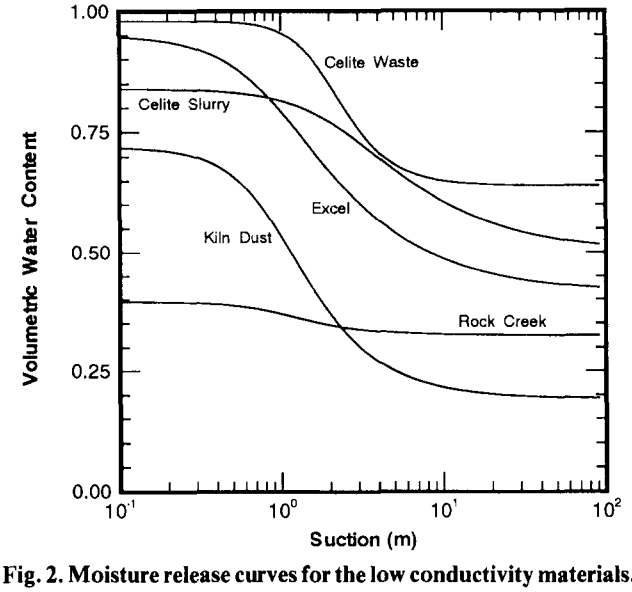

Fig. 2. Moisture release curves for the low conductivity materials.

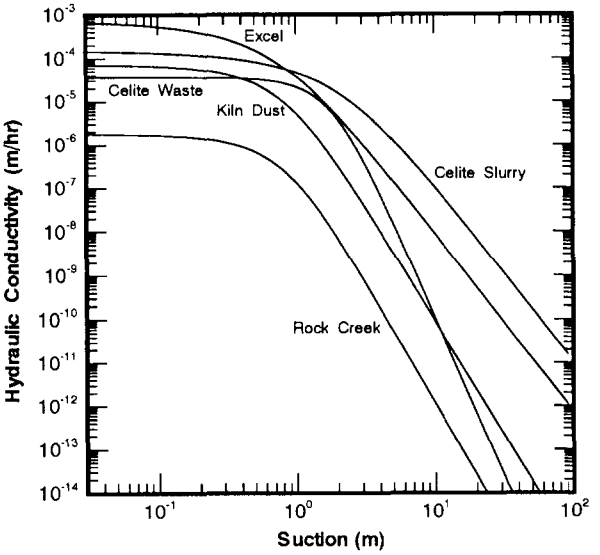

Fig. 3. Hydraulic conductivity curves for the low conductivity materials.

center nodes along the top boundary to simulate migration of leachate from the liner to the underlying materials. Several different flow rates were used to examine their effects on the performance of the liner. Employing the unit gradient boundary condition at the bottom of the coarse layer is analogous to considering the coarse layer to be of infinite vertical extent.

Results

Results of the numerical experiments, simulating the performance of the liners under various leakage conditions, are analyzed and discussed in the following sections. The effects of different clay-like material, its thickness, and the leakage rate on the lateral spreading along the interface were examined.

Effect of Thickness on Lateral Spreading

The thickness of the overlying low permeable layer is one of the important factors to be considered in the design of a liner system because it affects the arrival time of the leachate from the top of the liner to the interface with the coarse material as well as the degree of lateral migration. A liner that maximizes the arrival time and the degree of lateral spreading so that it can retard leachate migration and allow for a relatively sparse monitoring network is considered desirable.

Intuitively, as the thickness of the fine-textured layer is increased, the time for the front to reach the interface will increase. In turn, the lateral spreading of the front should increase as a result of the larger residence time (the time a water particle travels from the source to the interface of the second layer).

In order to quantify the relationship between thickness and lateral spreading, four simulations with different thickness for one of the low conductivity materials (Kiln Dust) were carried out. The thickness was varied from 0.15 to 1.22 meters. A sensitivity analysis was performed by comparing the numerical results obtained with different element size. The optimal spatial discretization of the liner for the first

three thicknesses consisted of 923 nodes and 840 finite elements (Figure 1). The finite-element grid for the simulation of the 1.22 meter thick, low conductivity layer consisted of 1492 nodes and 1400 elements. The vertical and horizontal distance between adjacent nodes was kept constant for these simulations, regardless of number of nodes and elements. The flux at the three central nodes was set equal to the saturated hydraulic conductivity of the Kiln Dust (Table 1) for all four simulations. Each simulation was extended until the time when the leachate front reached the interface. The leachate front (wetting front) was defined as the front where the moisture content increases 10% above the initial moisture content. Had a different definition of the wetting front been used, the absolute values for wetting front movement and time to reach the interface would have been different. However, the ratio of horizontal to vertical movement would still remain the same.

The ability of a given liner layer to retard vertical movement is directly related to the time it takes for the wetting front to reach the interface. Figure 4 presents the time to reach the interface as a function of the thickness. From this figure, it is clear that this time is related to the thickness in a quadratic fashion.

The relationship between lateral spreading along the top boundary (measured from a line bisecting the constant flux source) and the vertical movement is depicted in Figure 5. This figure indicates that the lateral spreading is about 80% of the vertical movement along the low conductivity layer (Kiln Dust) by the time that the wetting front reaches the interface. The difference between horizontal and vertical movement is the result of the gravity pull. For the other four materials, it is expected that the relationship between the vertical and horizontal movement will also be linear, although the proportionality constant may be different. This relationship helps to determine how much spreading will occur before the wetting front completely penetrates the low conductivity layer.

The results of these four simulations indicate that

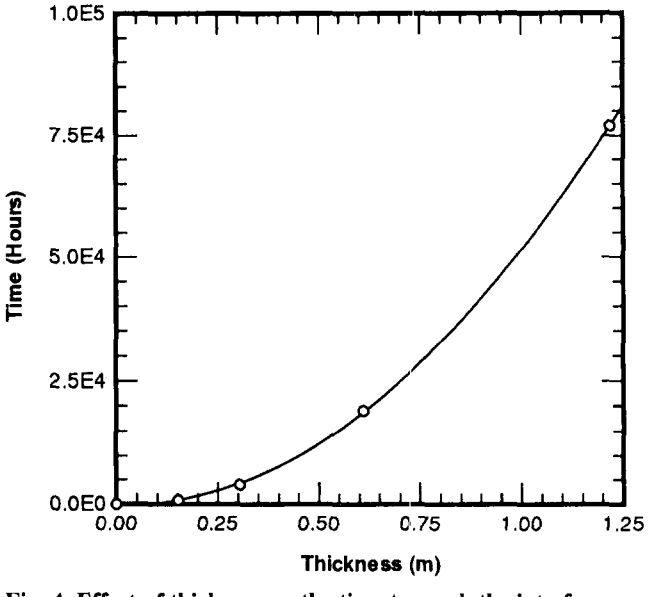

Fig. 4. Effect of thickness on the time to reach the interface.

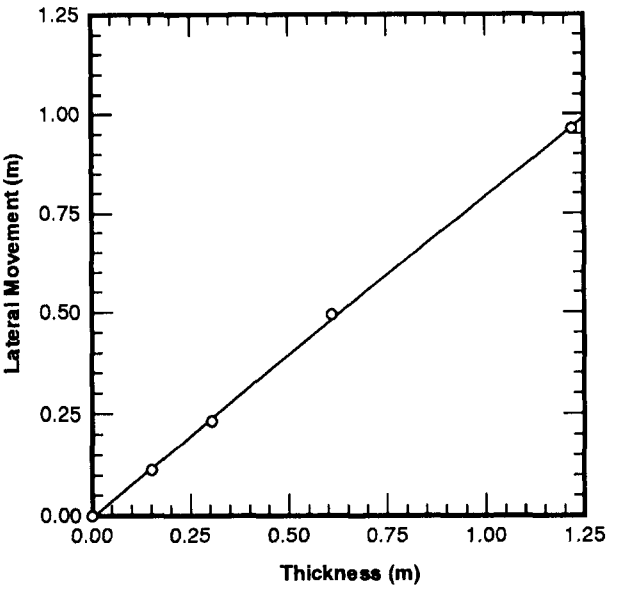

Fig. 5. Lateral spreading along the top boundary as a function of thickness.

doubling the thickness of the low conductivity layer will double the lateral spreading along the top; however, the time to reach the interface will be at least four times greater. For monitoring purposes, these results imply that a thick layer will increase the travel time while allowing larger distances between monitoring locations. Thus, actual liner thickness at the site should be as large as possible and only limited by engineering and economic constraints.

Wicking Ability of the Five Candidate Materials

The quadratic relationship between layer thickness and time to reach the interface (Figure 4), and the linear relationship between lateral spreading and the vertical movement (Figure 5) suggest that, if the lateral spreading (L) is plotted as L^2 versus time, a linear relationship should be obtained. This behavior, as expected based on the nature of equation (3), is typical of diffusion controlled processes. Since the spreading of the leachate front is governed by a diffusion-like process, it is easy to visualize the phenomenon for times prior to the front contacting the interface. After the contact the same may not be true and the movement along the interface may or may not exhibit this behavior.

In order to further verify this behavior, two plots were prepared: one showing the relation between the square of lateral movement along the top boundary and the simulation time (Figure 6), and the other showing the square of the lateral movement along the interface as a function of time after the wetting front has reached such interface (Figure 7). Apparently, the square of the lateral movement, along both boundaries, top and interface, is linearly related to the time. These findings confirm that the lateral spreading is controlled by the diffusivity of the material. Based on this finding, it should suffice to compute the diffusivity for each of the five candidate materials, and then select the one with the maximum diffusivity within the matric potential range of interest.

To quantify the wicking ability of the five low conductivity materials, their diffusivity was computed as follows:

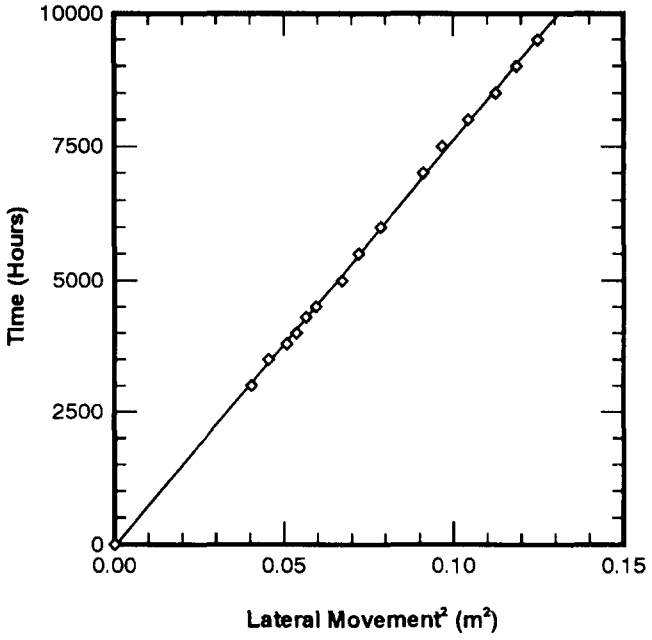

Fig. 6. Lateral movement along the top boundary as a function of time.

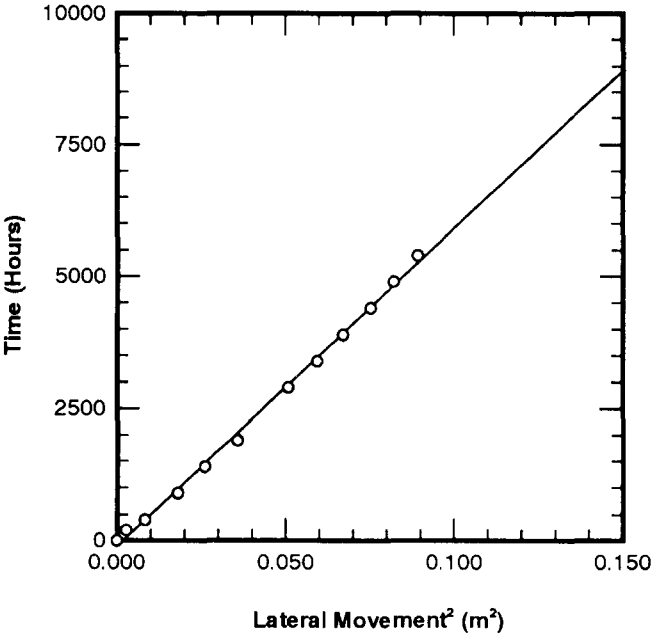

Fig. 7. Lateral movement along the interface as a function of time after contact.

$$D(\Psi) = \frac{K(\Psi)}{C(\Psi)} \qquad (4)$$

Figure 8 depicts the diffusivity as a function of matric potential for the five materials. One may postulate, based on this figure, that the lateral spreading in the Celite Slurry should be larger than that in the Rock Creek. The spreading in the Celite Waste, however, will be larger or smaller than that in the other four porous materials depending on the range of matric potential. For example, for matric potential values smaller than 0.30 meters, the spread in the Celite Waste will be larger than that in any of the remaining four materials. Nonetheless, as the matric potential increases, for example, from 0.30 to 3.0 meters, the spread in the Celite Waste may be less than that in the Celite Slurry, and as the matric potential approaches 3.0 meters, it may become less than that in the Excel.

Three additional simulations were conducted varying the material in the low conductivity layer to verify that the diffusivity function controls the migration of the wetting front. The materials used in these simulations were: Kiln Dust, Excel, and Celite Slurry. The finite-element grid was kept the same (923 nodes and 840 elements) for these simulations. The leakage rate at the top boundary was set equal to the saturated hydraulic conductivity of the Kiln Dust (7.32×10^{-5} m/hr). Under this leakage rate, the three materials remained under a state of partial saturation for the duration of the simulations.

The output of these simulations was analyzed in terms of the square of the lateral spreading as a function of simulation time in keeping with the diffusive nature of the spreading. The square of the lateral movement (L^2) along the interface versus time, after the wetting front has contacted the interface, is presented in Figure 9. This figure shows a clear linear relationship between L^2 and time after contact for the three different materials. From the abscissae of these lines, the Celite Slurry produces the maximum lateral spreading, followed by the Excel and then by the Kiln Dust as indicated by the magnitude of the diffusivity (Figure 8). However, the maximum spreading by 5,000 hours is only approximately 0.46 meters, and no breakthrough into the lower layer was observed even at times greater than 70,000 hours. The difference in diffusivity values seems to explain the result that the degree of spreading of the Excel is closer to that of Celite Surry than that of Kiln Dust. The difference between diffusivity values at a given matric potential is larger for the Kiln Dust and Excel than that for Excel and Celite Slurry.

The diffusivity function indicates that the material which maximizes the wicking effect, over a large range of matric potential, is the Celite Slurry. However, the material which minimizes the vertical movement for the given leak-

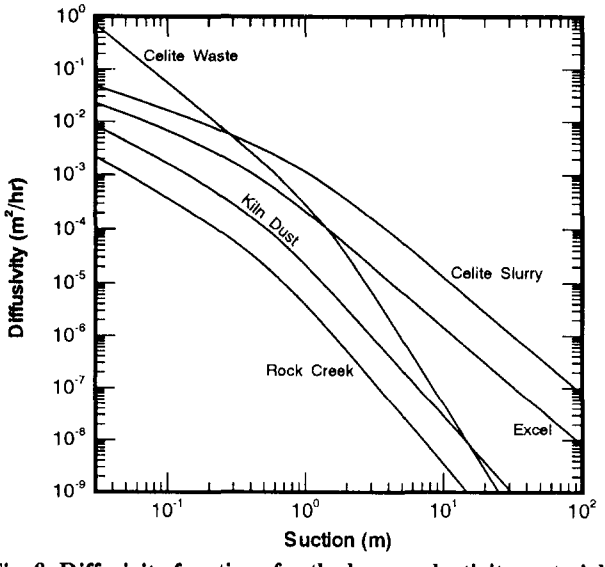

Fig. 8. Diffusivity functions for the low conductivity materials.

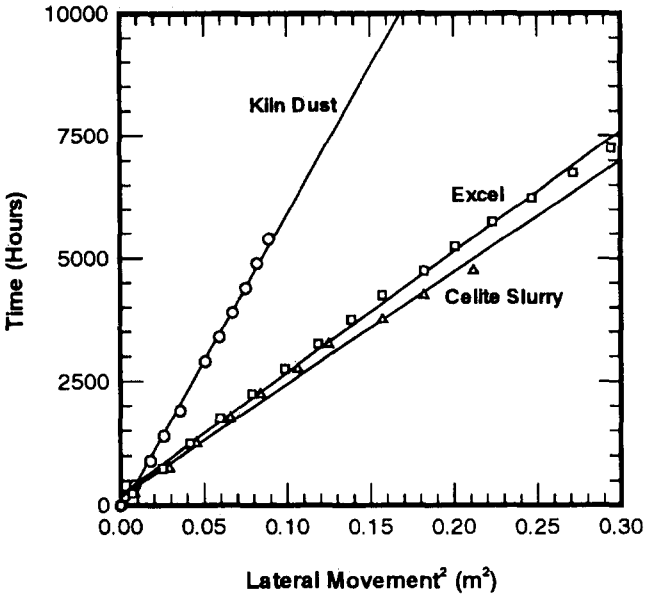

Fig. 9. Lateral movement of the wetting front as a function of time after contact.

Table 2. Time to Reach the Interface with Leakage Rate Equal to the Saturated Hydraulic Conductivity of the Kiln Dust

Material	*Time (hrs)*
Excel	2,750
Celite Slurry	5,250
Kiln Dust	19,100

age rate is the Kiln Dust (see Table 2). Therefore, if one desires to minimize the vertical movement of infiltrating water the material with the minimum conductivity should be selected (see Table 1). However, maximizing the wicking effect of a layer may result in unacceptably large vertical movement.

Effect of Leakage Rate on Wicking

Two sets of simulations were carried out with the three different materials to quantify the effects of leakage rate on the lateral spreading of the wetting front. In the first set of simulations the rate through the top boundary was set equal to the magnitude of the saturated hydraulic conductivity of each material, and in the other, equal to 20% of the saturated conductivity. The total infiltration volume for both sets of simulations was kept the same by running the second set of simulations five times longer than the first set. This constant infiltration volume allows the comparison of the degree of the migration at the end of the simulations. If the same simulation time were used, the set with a larger flow rate would show greater lateral spreading, thereby rendering the comparison meaningless. The degree of lateral migration as a function of leakage rate for the three different materials is illustrated in Figure 10. For the same total infiltration volume, a small flow rate produces larger lateral spreading than a larger flow rate. This is attributed to the fact that the time required to infiltrate the same volume with a small leakage rate is longer. Consequently, the opportunity for water to imbibe into a given material is enhanced.

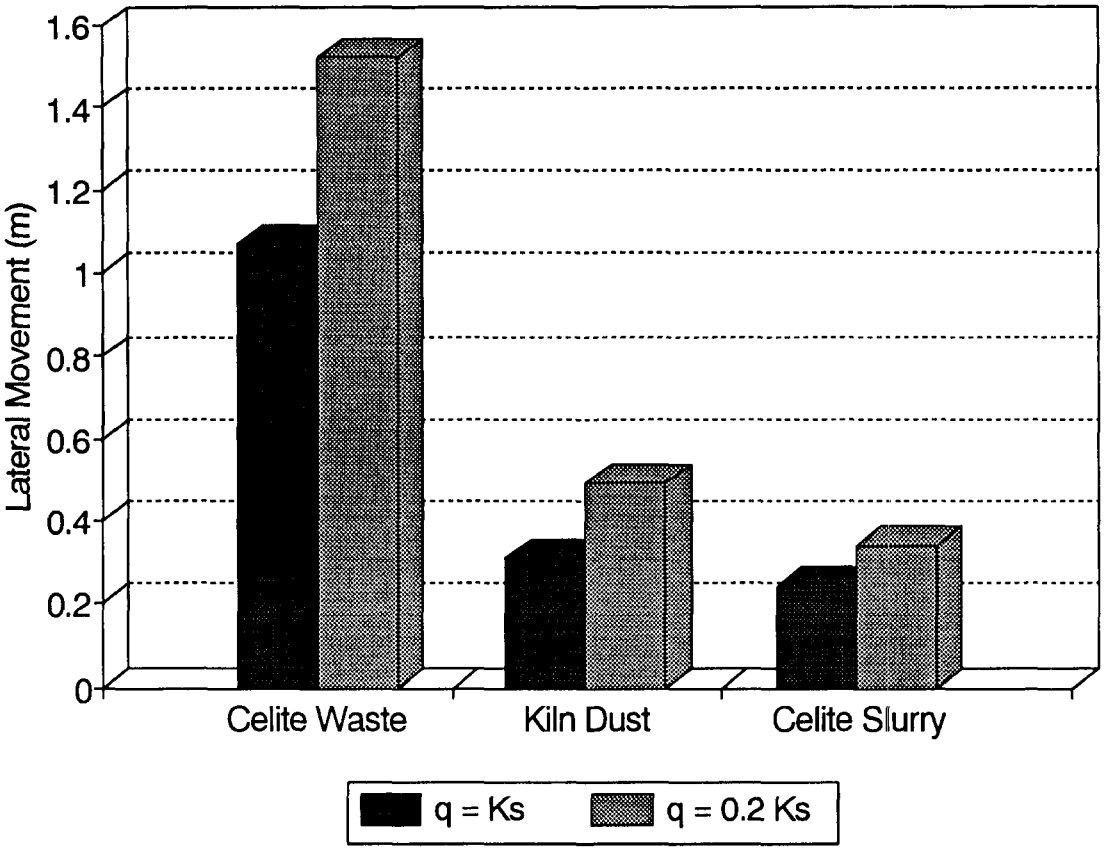

Fig. 10. Effect of the flow rate on the lateral migration.

Three-Layer System

The results of numerical simulations presented in previous sections demonstrate that a two-layer liner system consisting of a fine-textured (clay-like) material overlying a coarse-textured (sand-like) material will present both the capillary barrier and the wicking effect. However, the results also demonstrate that lateral wicking effect in such a two-layer system tends to be insignificant due to the small diffusivity value of the fine-textured material. Such a weak wicking effect may cause accumulation of leachate at the interface between the fine and coarse texture materials, which may eventually cause leachate migration into the coarse material and then into the underlying ground water. In addition, a closely spaced monitoring system will be required to detect any leakage due to the insignificant wicking effect. These findings indicate that a better design of the multilayer liner system is necessary.

An ideal multilayer linear system should minimize the vertical movement of leachate and maximize the lateral wicking effect. In order to meet these requirements, a three-layer liner system composed of a clay-like layer overlying a fine-sand-like layer on the top of a coarse-gravel-like layer is proposed. In this three-layer linear system, the clay-like layer will retard the vertical movement of the leachate. Any leakage at the interface between the clay-like and fine-sand-like layers should move rapidly through the fine-sand-like material and be retained at the interface between the fine-sand and coarse-gravel-like material. Since the diffusivity of the fine-sand-like material is large, the leachate at the interface should be quickly diverted laterally away from the source. As such, the three-layer liner system should have a significantly larger wicking effect capacity than the two-layer liner. To demonstrate this postulation, numerical experiments of flow through a three-layer liner were conducted and are discussed below.

Design of the Three-Layer Numerical Experiments

A two-dimensional cross section of a three-layer liner was used to study its wicking ability. The geometry of this cross section is presented in Figure 11 which also shows the finite-element discretization used for the numerical simulations. This grid is composed of 1680 elements and 1775 nodes. Element density was designed to be larger at areas where stronger pressure gradients were expected, resulting in a nonuniform grid. A sensitivity study of the effect of element size on the numerical results was carried out to determine the appropriate element size for the simulation. The dimensions of the cross section are 3.0 meters on the horizontal and 0.915 meters in the vertical, each layer being 0.305 meters in thickness. A slope of 3% was used to simulate the effect of a sloping liner bottom on the wicking ability.

The materials used for these simulations were: Chino Clay, a medium sand, and a coarse sand (Yeh and Harvey, 1990). The hydraulic properties for these materials are presented in Figures 12 and 13. Table 3 summarizes the Van Genuchten parameters for these materials. Figure 12 shows the relationship between volumetric water content and matric potential. At any given matric potential value, the

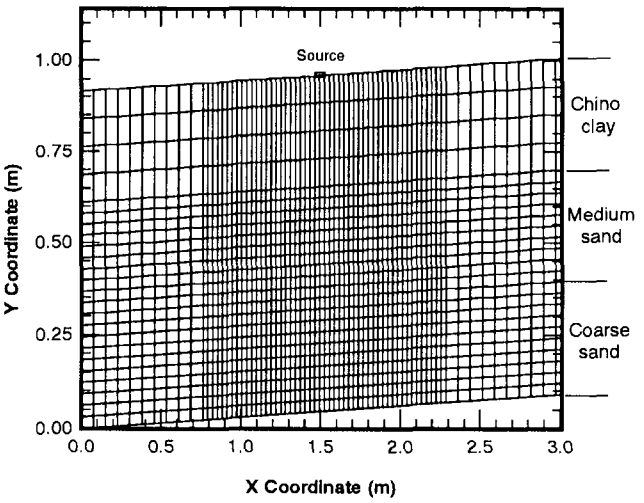

Fig. 11. Finite-element discretization of the three-layer liner cross section.

water content of the clay is larger than that of either sand. Figure 13 depicts the hydraulic conductivity as a function of matric potential for the three materials. The saturated hydraulic conductivities for the coarse and medium sand are of similar magnitude; however, as the matric potential increases, the conductivity of coarse sand decreases much faster than that of the medium sand. The saturated hydraulic conductivity of the Chino Clay is about three orders of magnitude smaller than that of either sand and the changes in conductivity are not as pronounced. Consequently, there exists a crossover point between the hydraulic conductivity of the clay and that of the sandy materials at a matric potential value of about 0.30 meters. At matric potential values higher than 0.30 meters, the hydraulic conductivity of the clay is larger than those of both sands.

Similar to the two-layer cases, initial conditions within the materials were assigned to represent static conditions in which no water movement takes place. A uniform total head

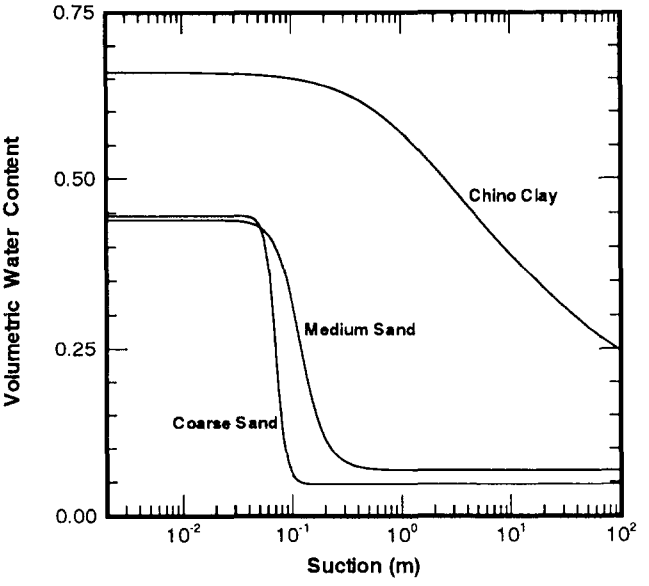

Fig. 12. Hydraulic conductivity as a function of suction for the three-layer system.

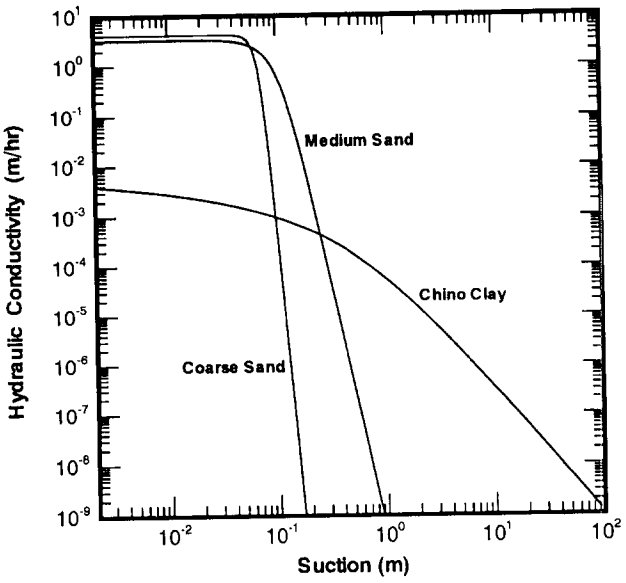

Fig. 13. Moisture release curves for the three-layer system.

Table 3. Unsaturated Hydraulic Parameters

Soil	Ks (m/hr)	α (1/m)	n (L°)	θ_s (L°)	θ_r (L°)
Chino Clay	8.25×10^{-3}	1.352	1.20	0.660	5×10^{-5}
Medium Sand	$0.326 \times 10^{+1}$	9.127	4.27	0.440	0.067
Coarse Sand	$0.405 \times 10^{+1}$	14.30	10.16	0.446	0.047

of −10.0 meters was assigned. Boundary conditions were prescribed as follows: unit gradient at the bottom nodes of the cross section, no-flow along the vertical sides of the liner and along the top except at the three source nodes located right at the center. At these nodes, a flux of 5.79×10^{-3} m/hr, which is about 70% of the saturated hydraulic conductivity of the Chino Clay, was prescribed.

Results

The numerical model was run until a total simulation time of 480 hrs. The resulting pressure profiles at selected times are shown in Figures 14(a) to 14(e). Evolution of the pressure disturbance is clearly shown in these figures. For instance, the pressure distribution after 60 hours [Figure 14(a)] depicts the retarding effect of the material interface between the clay and the fine sand, as indicated by the flattening of the contours near the interface (at about 0.61 meter elevation). As time progresses, the pressure disturbance propagates through the second layer and, by 216 hours, it has reached the second interface and its vertical movement is further retarded. From Figure 14(e), which shows the pressure contours at 360 hours, it is evident that the vertical no-flow boundaries are already restricting the lateral movement of the pressure pulse. The moisture profiles corresponding to the pressure distributions of Figures 14(a) to 14(e) are shown in Figures 15(a) to 15(e). A comparison of Figures 14(d) and 15(d) shows the difference in penetration of the wetting and pressure fronts at a simulation time of 216 hours. At this time, the pressure pulse is already spreading within the second layer and has also reached the second interface. However, there is very little

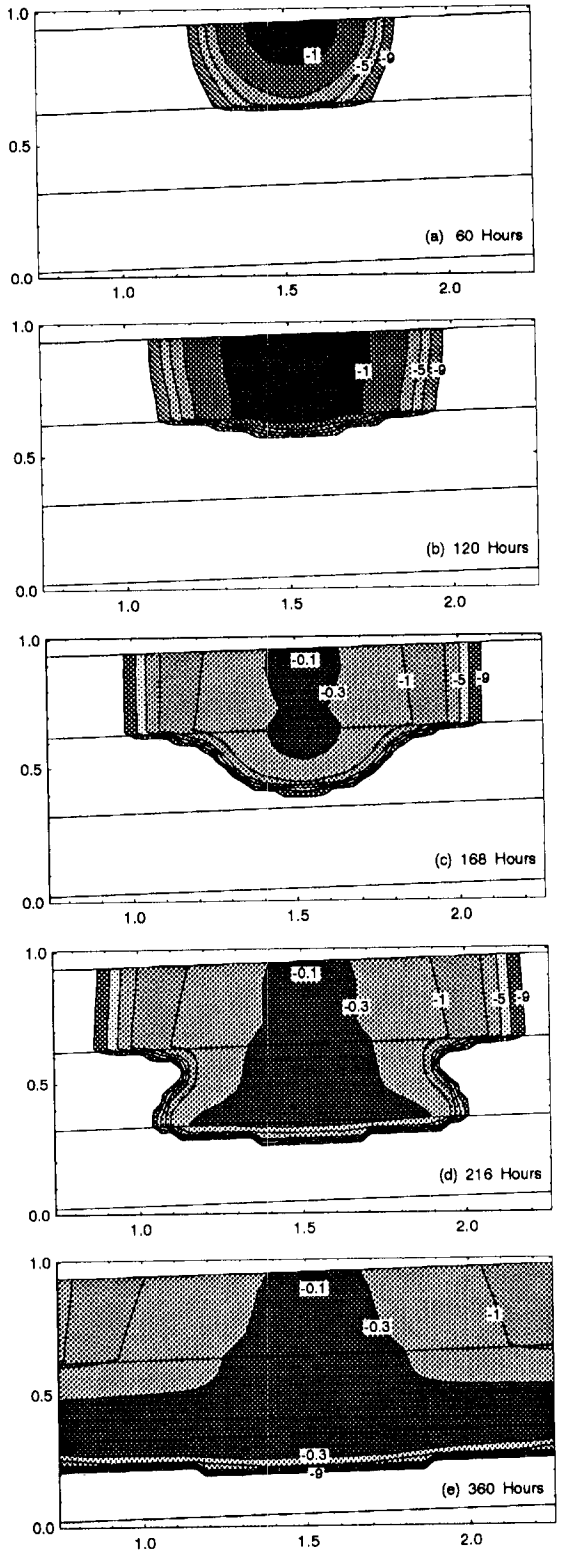

Fig. 14. Matric potential distribution at different times: (a) 60; (b) 120; (c) 168; (d) 216; (e) 360 hours.

penetration of the moisture front in the second layer. By the simulation time of 360 hours [Figure 15(e)], the effect of the second interface on the wetting front is quite pronounced and the strong wicking effect of the three-layer liner, as indicated by the large lateral movement of the wetting front in the second layer, is evident.

In order to compare the lateral movement within the first and the second layer Figure 16 was prepared. In this

figure, the lateral movement of the wetting front along the bottom of the clay and the medium sand layers was plotted as a function of time. The wetting front was defined as the contour corresponding to a 10% increase over the initial water content in either layer. The solid line in Figure 16 indicates that the wetting front within the clay moves laterally about 0.75 meters in 360 hours, whereas that in the

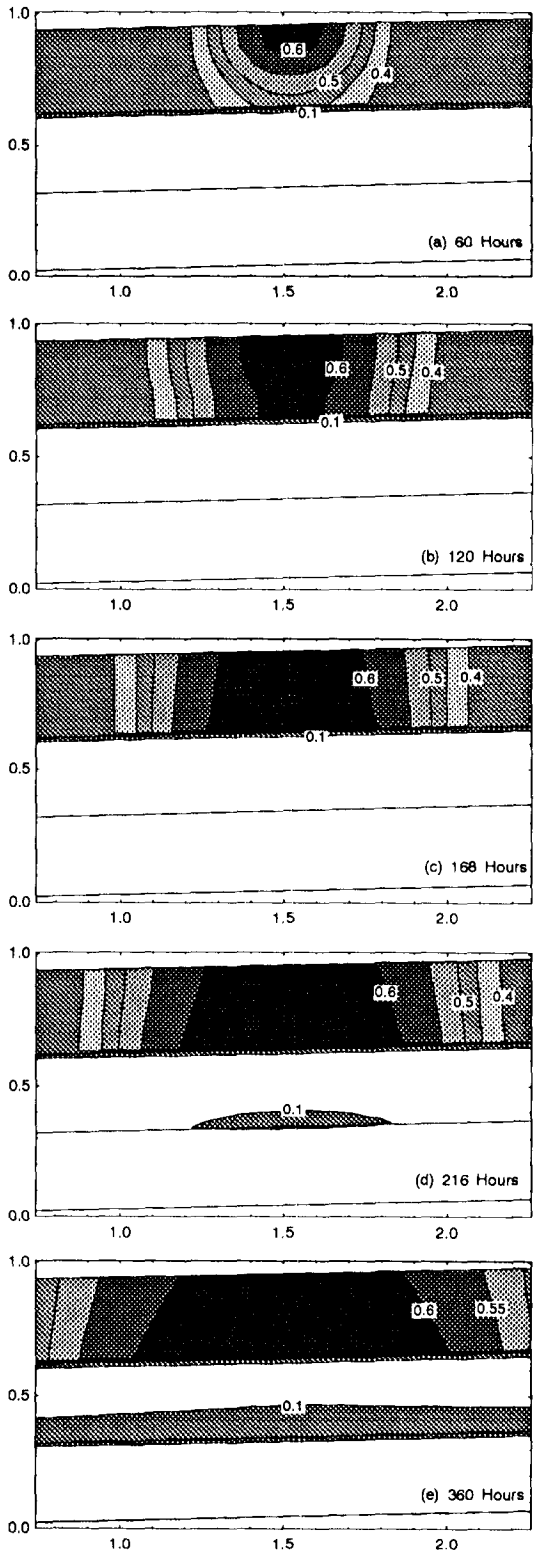

Fig. 15. Matric potential distribution at different times: (a) 60; (b) 120; (c) 168; (d) 216; (e) 360 hours.

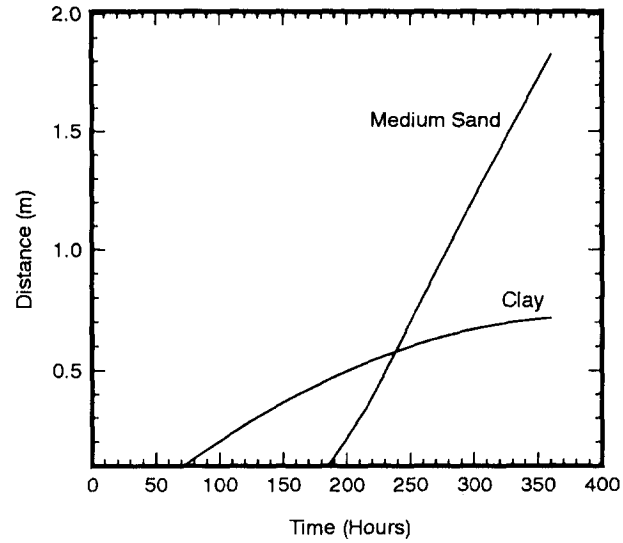

Fig. 16. Lateral movement of the wetting front in clay and medium sand.

medium sand moves more than 1.50 meters in the same time. Moreover, the rate of lateral speading in the clay decreases with time while that in the sand remains almost constant.

Profiles along a vertical line bisecting the source are depicted in Figures 17(a) and (b) respectively to visualize the behavior of the pressure and wetting fronts within the medium sand. The pressure pulse reaches the second interface between 168 and 216 hours. The change in pressure at any given point along the interface during this period is "abrupt," from about -6.1 meters to greater than -0.3 meters. From then on, the pressure at the interface changes at a smaller rate; however, the water content changes rapidly.

Conclusion

Performance of hypothetical two- and three-layer liner systems was evaluated using numerical simulations. Based on the simulation results, we can conclude that a safer liner may be constructed by using a three-layer system composed of a layer of fine-sand-like material which has high diffusivity values in between a top layer of a thick low conductivity, clay-like material and a bottom layer of a high conductivity material. Some apparent advantages of such a three-layer system over the two-layer system are: (1) Monitoring, as required by regulatory agencies, can be achieved with a relatively sparse sampling network along the intermediate sand-like layer. The time to collect a meaningful sample can be dramatically reduced. (2) Such a system also lessens the possibility of leachate penetrating the second interface as a result of capillary barrier effect of the coarse material below and the wicking effect due to the large diffusivity of the fine-sand-like material. Any leachate reaching this interface will quickly spread laterally in the middle layer due to its relative higher diffusivity, as compared to that of the clay layer. (3) Any preferential flow (such as flow along cracks and fingers arising from instability) would be quickly diverted laterally as explained above and easily detected by the monitoring network.

Results of the simulations for the two-layer linear sys-

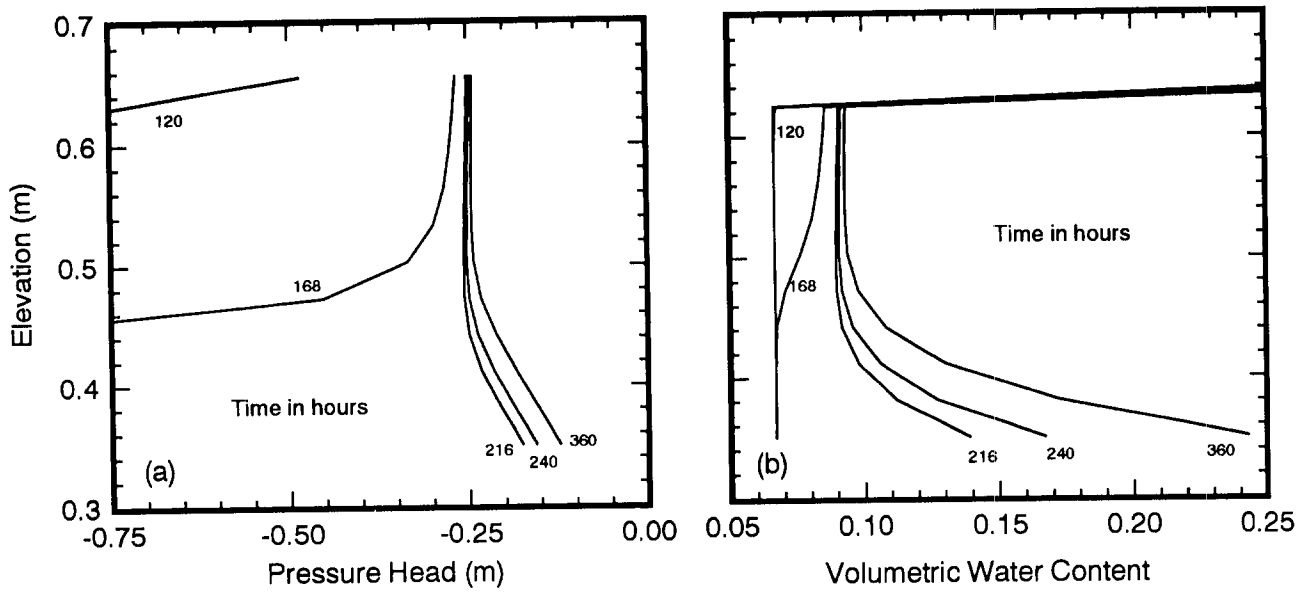

Fig. 17. Profiles along a vertical line through the source: (a) pressure; and (b) moisture.

tem indicated that the ratio of the vertical to horizontal movement of the wetting front before reaching the interface is constant with time. It was also found that doubling the thickness of the low conductivity layer doubles the lateral spreading along the top, and that the time to reach the interface increases in a quadratic fashion as a function of the thickness. The quadratic relationship between the thickness and time to reach the interface illustrates the diffusive nature of the leakage movement within the low conductivity layer. Therefore, it will suffice to use the diffusivity of the candidate materials as a criterion for selecting the one which may produce the maximum wicking effect.

Acknowledgment

Funding for this study was provided by Waste Management of North America, Inc.

References

Bear, J. 1972. Dynamics of Fluids in Porous Media. American Elsevier Publishing, Inc., New York. 764 pp.

California Administrative Code. Title 23, Chapter 3, Subchapter 15, Article 15.

Frind, E. O., R. W. Gillham, and J. F. Pickens. 1977. Application of unsaturated flow properties in the design of geologic environments for radioactive waste storage facilities. In: Finite Element Simulation Surface and Subsurface Hydrology. G. Pinder and W. Gray, eds. Academic Press, NY. 3.133-3.163.

Gagnard, P. E., T.-C.J. Yeh, R. Srivastava, A. Guzman, and J. Kramer. 1993. Numerical simulations on a two layer-liner system. Waste Management and Research. Under review.

Geswein, A. J. 1975. Liners for land disposal sites: An assessment. U.S. Environmental Protection Agency, EPA/530/Sw-137.

Haxo, H. E., Jr, R. S. Haxo, N. A. Nelson, P. D. Haxo, R. M. White, S. Dakessian, and M. A. Fong. 1985. Liner Materials for Hazardous and Toxic Wastes and Municipal Solid Waste Leachate. Noyes Publications, Park Ridge, NJ. 435 pp.

Hillel, D. 1971. Soil and Water: Physical Principles and Processes. Academic Press, NY. 288 pp.

Istok, J. 1989. Groundwater Modeling by the Finite Element Method. Water Resources Monograph 13. American Geophysical Union, Washington, DC. 495 pp.

Johnson, T. M., K. Cartwright, B. L. Herzog, and T. H. Larson. 1983. Modeling of moisture movement through layered trench covers. In: Role of the Unsaturated Zone in Radioactive and Hazardous Waste Disposal. J. W. Mercer, P.S.C. Rao, and I. W. Marine, eds. Ann Arbor Science, MI. pp. 11-26.

McWhorter, D. B., J. D. Nelson, T. A. Shepherd, and R. E. Wardwell. 1983. Role of partially saturated soil in liner design for hazardous waste disposal sites. In: Role of the Unsaturated Zone in Radioactive and Hazardous Waste Disposal. J. W. Mercer, P.S.C. Rao, and I. W. Marine, Ann Arbor Science, MI. pp. 81-100.

Mualem, Y. 1976. A Catalog of the Hydraulic Properties of Unsaturated Soils, Development of Methods, Tools and Solution for Unsaturated Flow with Application to Watershed Hydrology and Other Fields. Research Project 442, Technion Israel Institute of Technology, Haifa, Israel.

Ross, B. 1990. The diversion capacity of capillary barriers. Water Resources Research. v. 26, no. 10, pp. 2625-2629.

van Genuchten, M.Th. 1978. Calculating the Unsaturated Hydraulic Conductivity with a New Closed-Form Analytical Model. Research Report No. 78-WR-08. Princeton Univ., NJ.

Yeh, T.-C.J., L. W. Gelhar, and A. L. Gutjahr. 1985. Stochastic analysis of unsaturated flow in heterogeneous soils. 3. Observations and applications. Water Resources Research. v. 21, no. 4, pp. 465-471.

Yeh, T.-C.J. and D. J. Harvey. 1990. Effective unsaturated hydraulic conductivity of layered sands. Water Resources Research. v. 25, no. 6, pp. 1271-1279.

Yeh, T.-C.J. and R. Srivastava. 1990. VSAFT2: Variably Saturated Flow and Transport in 2-Dimensions. A Finite Element Simulator. Dept. of Hydrology and Water Resources, Univ. of Arizona, Tucson. Technical Report No. HWR 90-010. 143 pp.

Yeh, T.-C.J., R. Srivastava, A. Guzman, and T. Hater. 1993. A numerical model for water flow and chemical transport in variably saturated porous media. Ground Water. v. 31, no. 4, pp. 634-644.

Zaslavsky, D. and G. Sinai. 1981. Surface hydrology: IV-flow in sloping, layered soil. Journal of the Hydraulics Division. v. 107, no. hyl, pp. 53-64.